Supporting Information (SI)

Dual-sensitized luminescent Eu(III) dosimeter for selective detection of inorganic phosphate *via* ligand displacement mechanism

Nitin Shukla[a], Juhi Sayala[a], Zafar Abbas[a], Ashis K. Patra[a]*

[a]Department of Chemistry, Indian Institute of Technology Kanpur, Kanpur 208016, Uttar Pradesh, India

E-mail: akpatra@iitk.ac.in

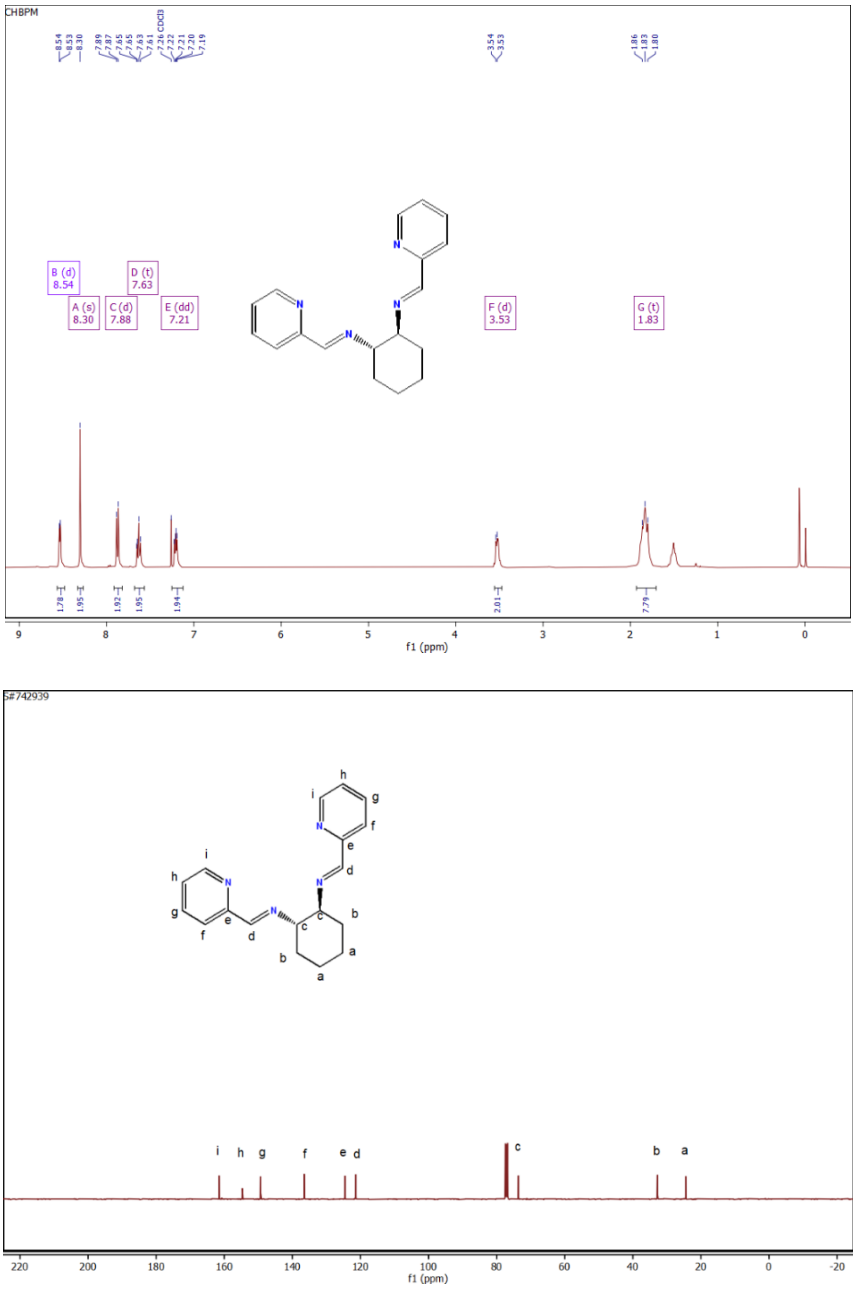

Fig. S1 ^{1}H and ^{13}C NMR spectra of L^{N4} ligand recorded in $CDCl_3$ in 400 MHz at 298K.

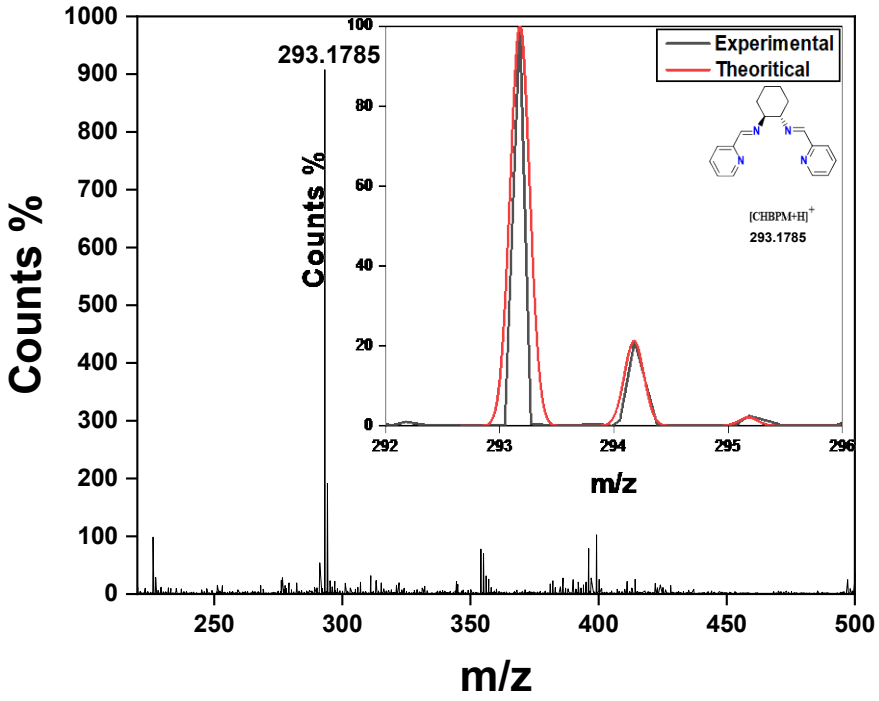

Fig. S2 ESI-MS spectra of the $\mathbf{L^{N4}}$ in $CHCl_3$ showing observed molecular ion peak as $[M+H]^+$ at *m/z* 293.1785. Inset shows the Experimental isotopic modeling (Black) with a matching theoretically predicted isotopic distribution profile (Red).

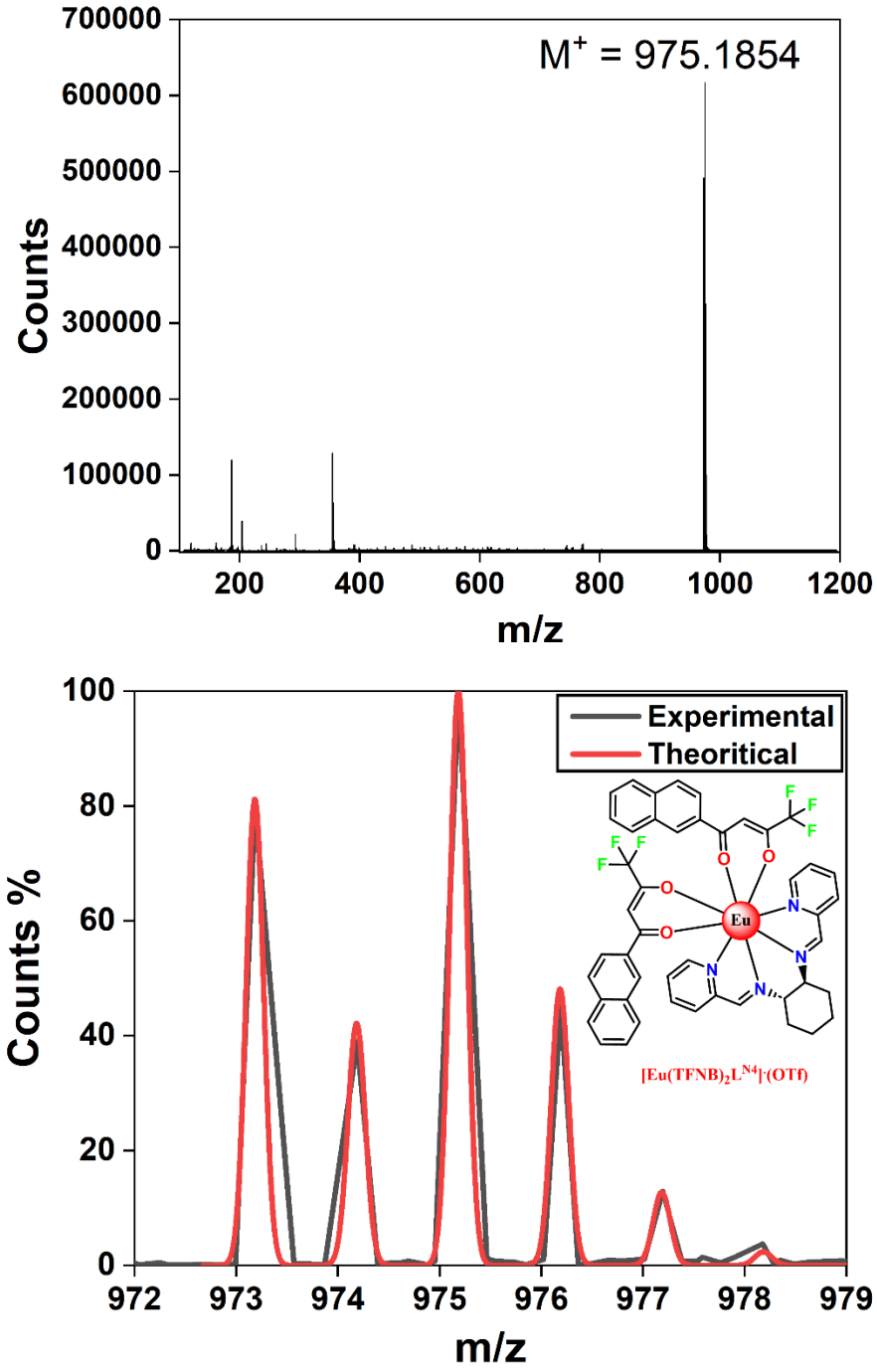

Fig. S3 ESI-MS spectra of the $[Eu(TFNB)_2L^{N4}](OTf)$ **(Eu.1)** in MeCN showing observed molecular ion peak as $[M]^+$ at *m/z* 975.1854 (black) with matching theoretically predicted isotopic distribution profile (red).

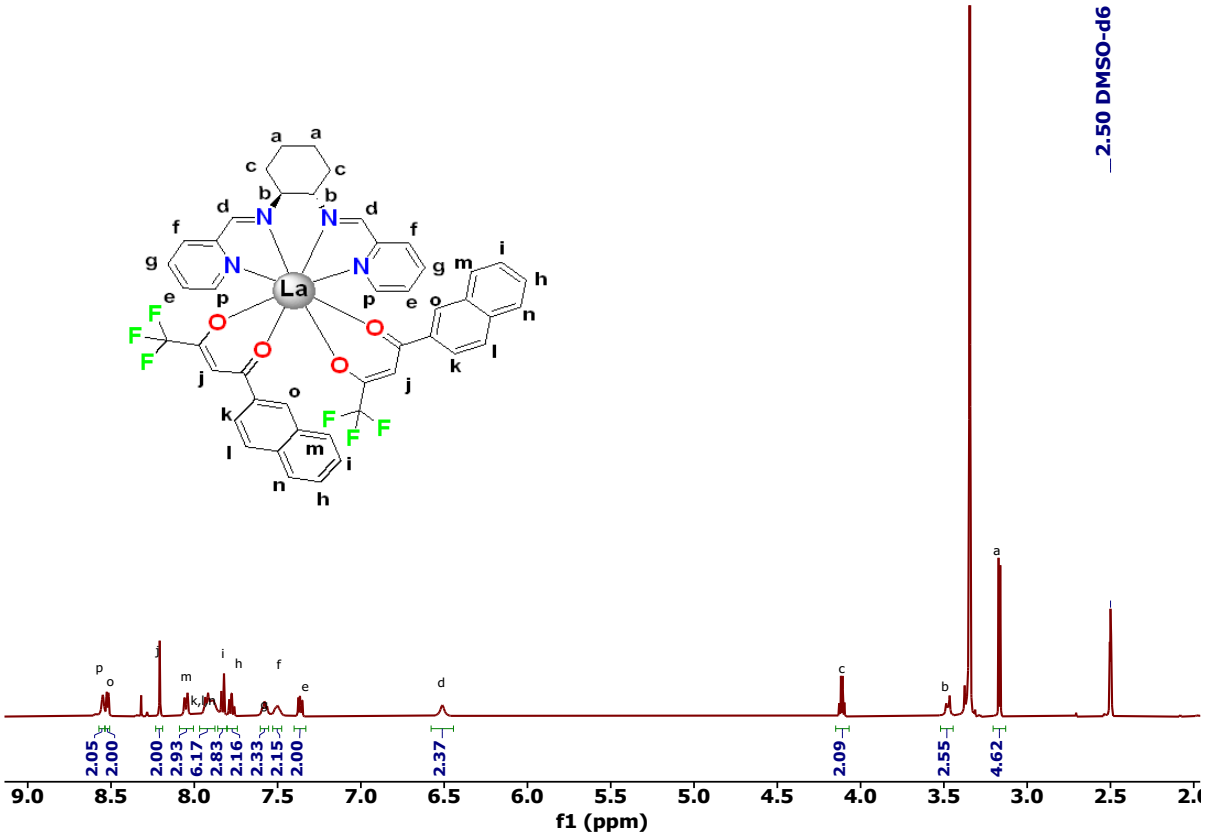

Fig. S4 ^{1}H NMR for **La.1**, a diamagnetic homologous lanthanide complex for solution state speciation in DMSO-d_6 in 400 MHz at 298 K.

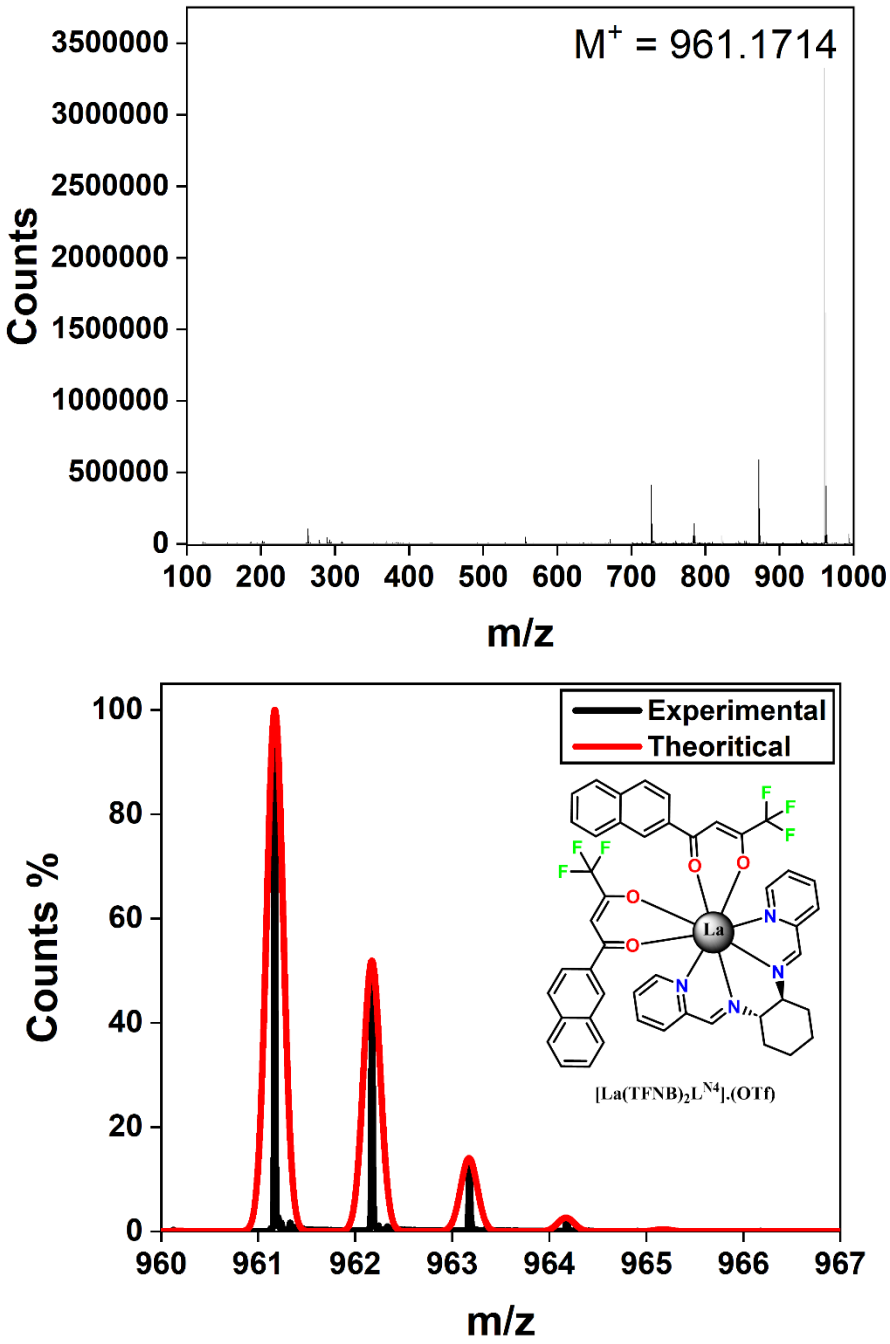

Fig. S5 ESI-MS spectra of the **[La(TFNB)$_2$L^{N4}](OTf) (La.1)** in MeCN showing observed molecular ion peak as $[M]^+$ at *m/z* 961.1714 (black) with matching theoretically predicted isotopic distribution profile (red).

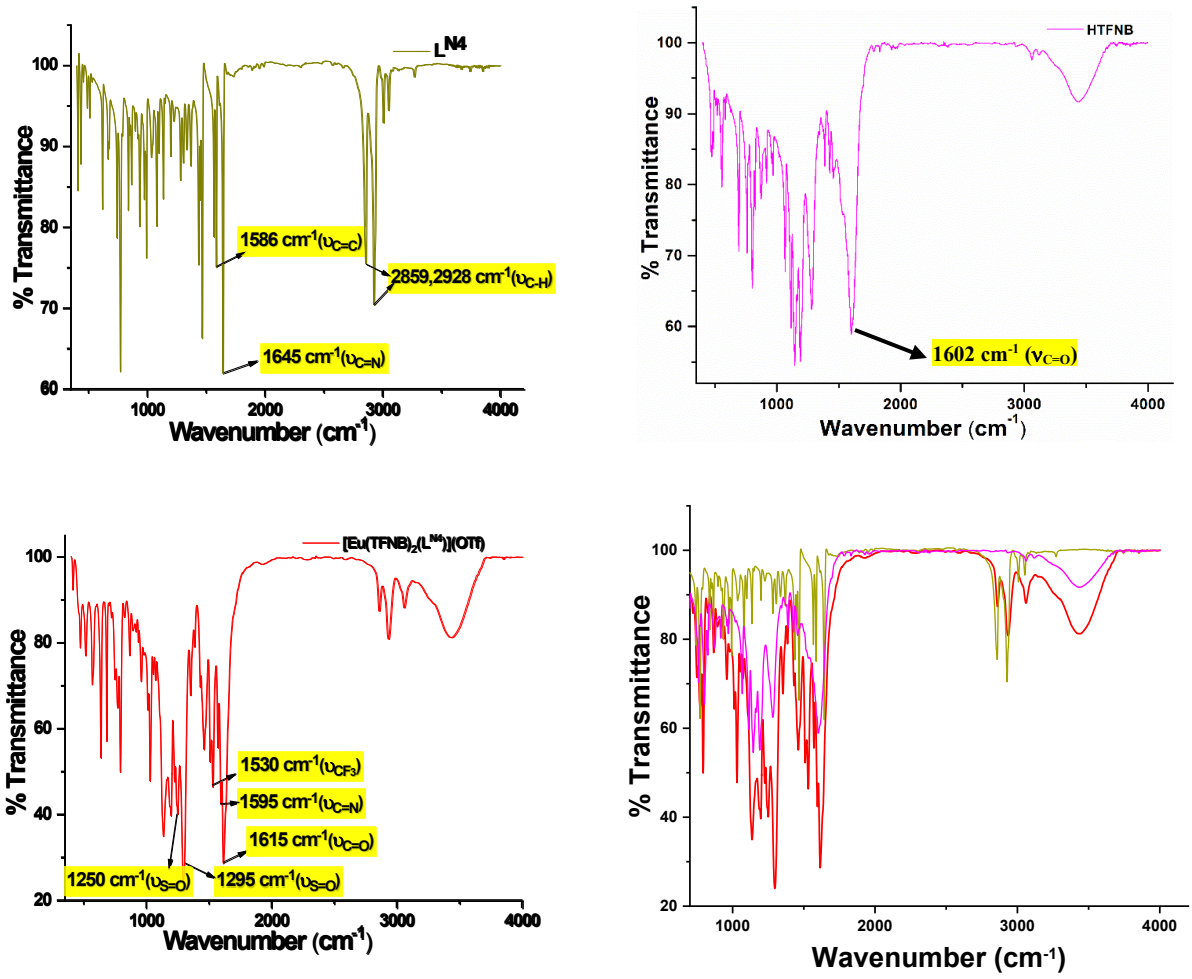

Fig. S6 FT-IR spectra of the (**a**) L^{N4} Ligand; (**b**) HTFNB antenna (anion, neutralized using equiv. moles of NaOH); (**c**) **Eu.1**; (**d**) merged spectra with vibration bands in the fingerprint regions in solid states (KBr pellets).

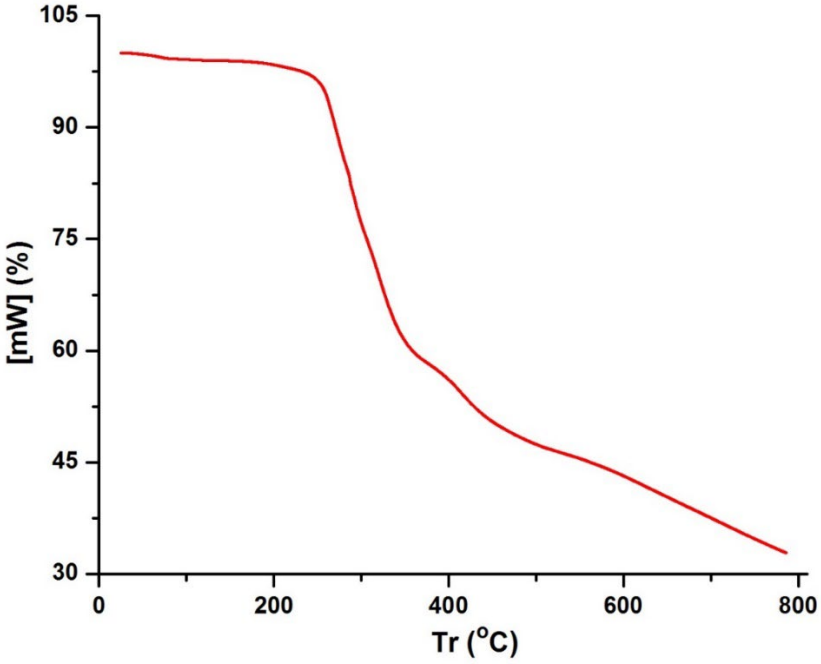

Fig. S7 TGA of complex **Eu.1** showing the stability of complex till 250°C after which there is an approx. 40% loss of mass owing to dissociation of ligand L^{N4}.

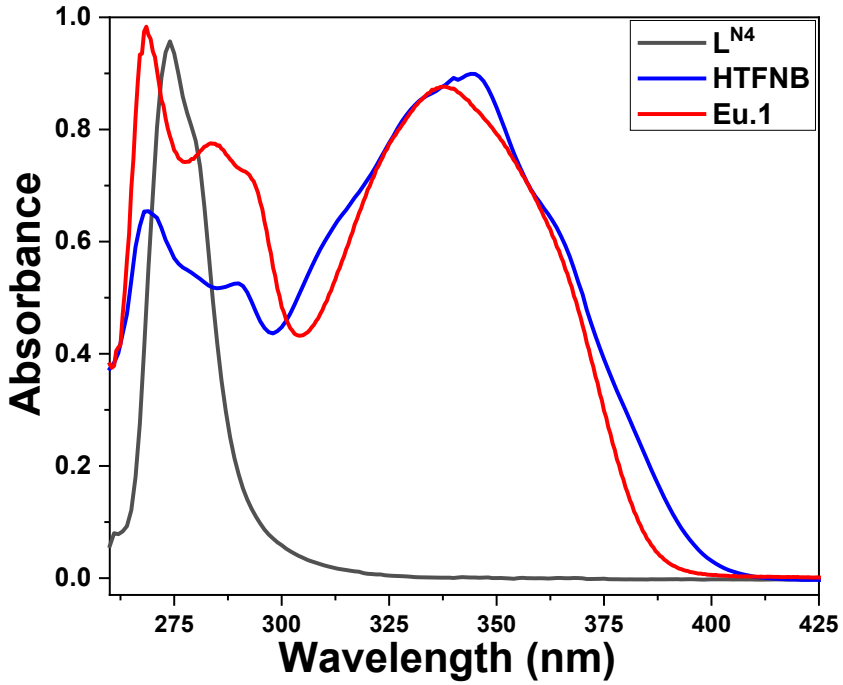

Fig. S8 Electronic absorption spectra of the ligands L^{N4} [7.5 μM] **(Black),** HTFNB [7.5 μM] **(blue)** and **Eu.1** complex [15 μM] **(Red)**, in MeCN at 298 K (All spectra are normalized).

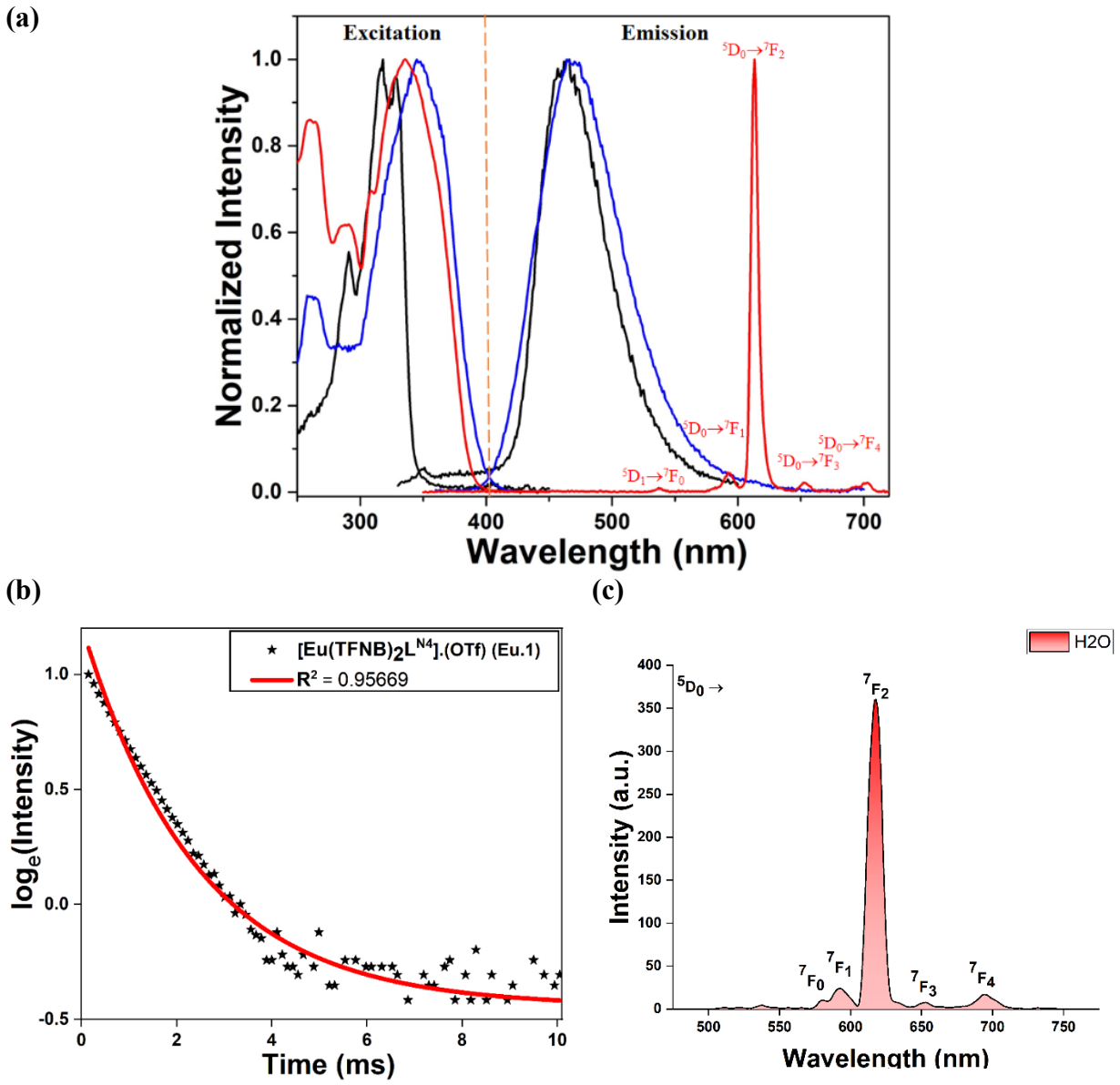

Fig. S9 (a) Excitation spectra of **Eu.1** complex and ligands (L^{N4} (10 µM) (black), HTFNB (20 µM) (blue) and [Eu(TFNB)$_2$$L^{N4}$](OTf) (10 µM) (red)) recorded at λ_{em}=470 nm for the ligands and λ_{em} = 613 nm ($^5D_0\rightarrow{}^7F_2$) for the complex and their respective photoluminescence spectra (λ_{ex} = 275 nm for L^{N4}, 344 nm for HTFNB and 340 nm for complex **Eu.1**). **(b)** Luminescence decay profile of $^5D_0\rightarrow{}^7F_2$ (lifetime measurements) for **Eu.1** in MeCN, $\lambda_{ex.}$ = 340 nm and $\lambda_{em.}$ = 613 nm with delay time and gate time = 0.5 ms, total decay time = 10.0 ms, Ex. and Em. Slit width = 5 nm each at 298 K. **(c)** Emission from **Eu.1** recorded in MeCN:Water–75:25 (v/v), delay time and gate time = 0.5 ms and Em. Slit width = 5 nm each at 298 K.

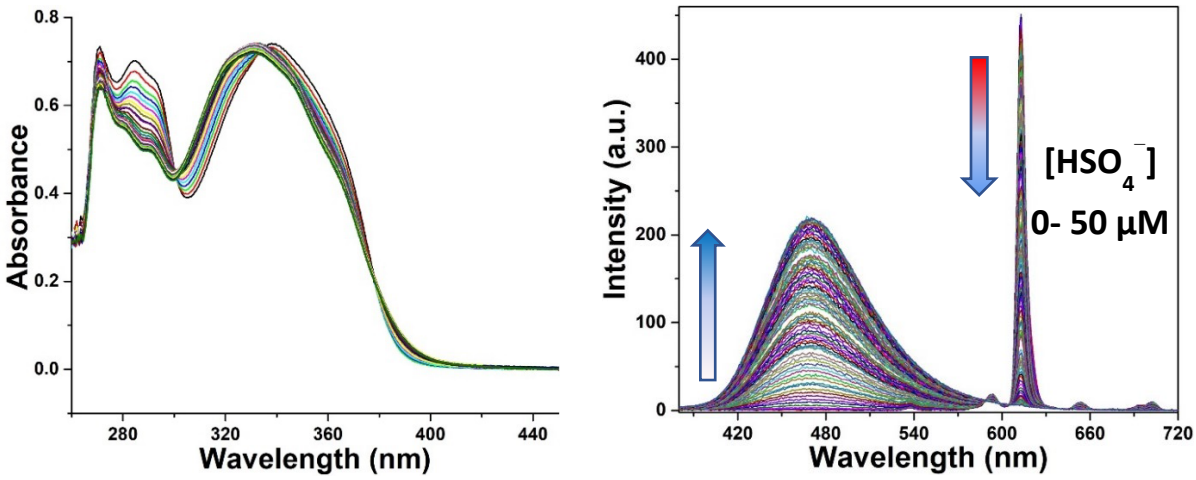

Fig. S10 Change in absorption spectra **(a)** and in the PL spectra **(b)** of **Eu.1** (2.5 µM) in MeCN with the increasing concentration of **[HSO_4^-]** in H_2O (0-50 µM) observed at characteristic emission bands of Eu(III) ion ($^5D_0 \rightarrow {}^7F_{J=0,1,2,3,4}$), λ_{ex} = 340 nm, ex. and em. slit width 5 nm.

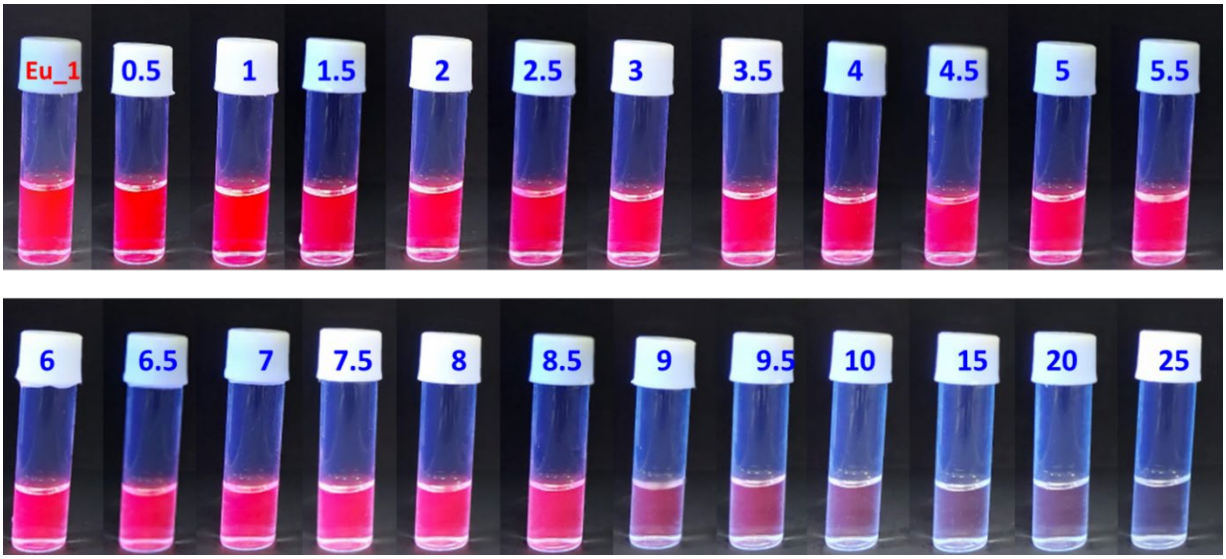

Fig. S11 Change in the emission of **Eu.1** (10 µM) in MeCN with the increasing concentration of **[HSO_4^-]** in H_2O (0-250 µM, 0-25 equiv.) as seen from the naked eye under UV light (365 nm).

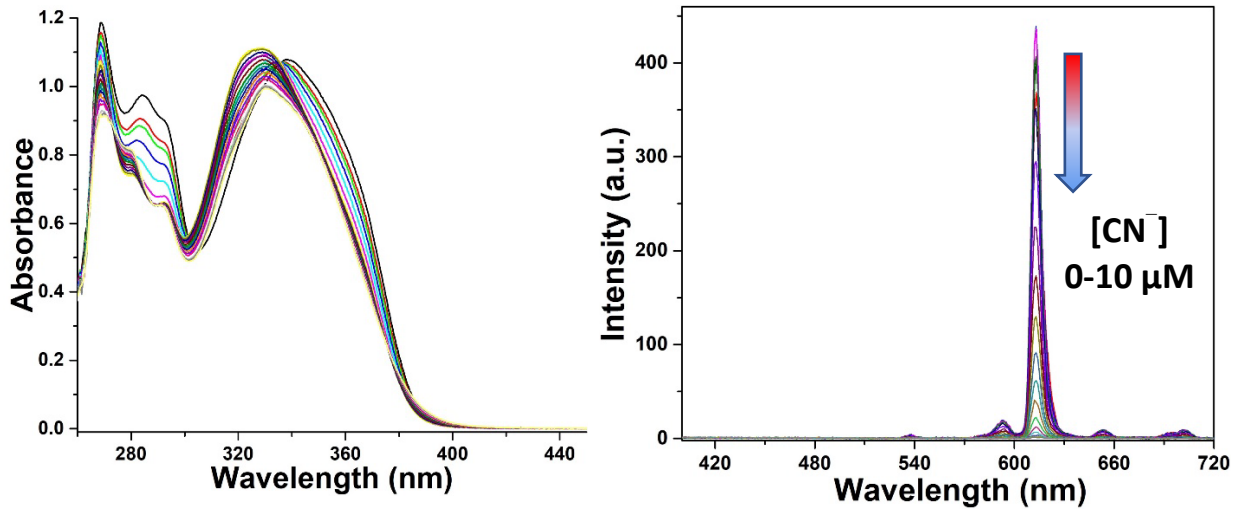

Fig. S12 Change in absorption spectra **(a)** and in the PL spectra **(b)** of **Eu.1** (2.5 µM) in MeCN with the increasing concentration of **[CN⁻]** (0-10 µM) in H_2O observed at characteristic emission bands of Eu(III) ion ($^5D_0 \rightarrow {}^7F_{J=0,1,2,3,4}$), λ_{ex} = 340 nm, ex. and em. slit width 5 nm.

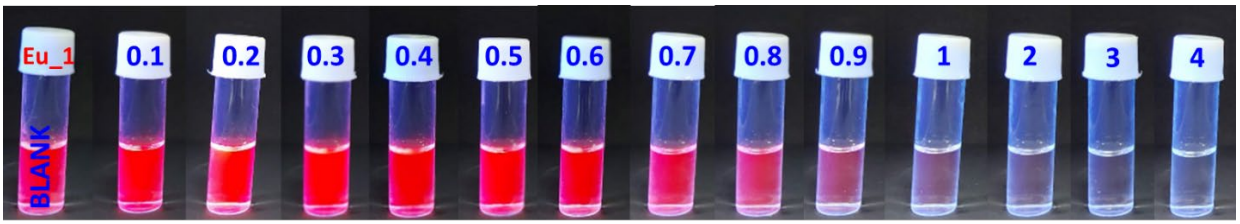

Fig. S13 Change in the emission of **Eu.1** (10 µM) in MeCN with the increasing concentration of **[CN⁻]** (0-40 µM, 0-4 equiv.) in H_2O as seen from the naked eye under UV light (365 nm).

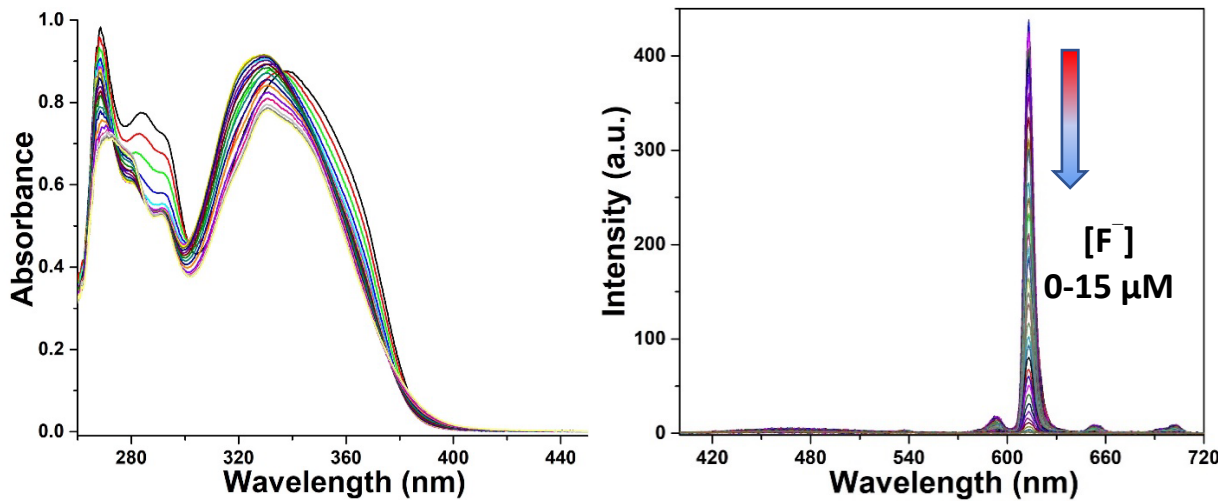

Fig. S14 Change in absorption spectra **(a)** and in the PL spectra **(b)** of **Eu.1** (2.5 µM) in MeCN with the increasing concentration of **[F⁻]** (0-15 µM) in H_2O observed at characteristic emission bands of Eu(III) ion ($^5D_0 \rightarrow {}^7F_{J=0,1,2,3,4}$), λ_{ex} = 340 nm, ex. and em. slit width 5 nm.

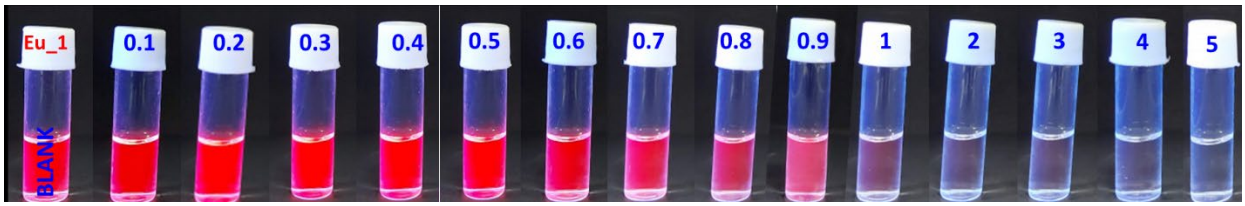

Fig. S15 Change in the emission of **Eu.1** (10 µM) in MeCN with the increasing concentration of **[F⁻]** in H_2O (0-50 µM, 0-5 equiv.) as seen from the naked eye under UV light (365 nm).

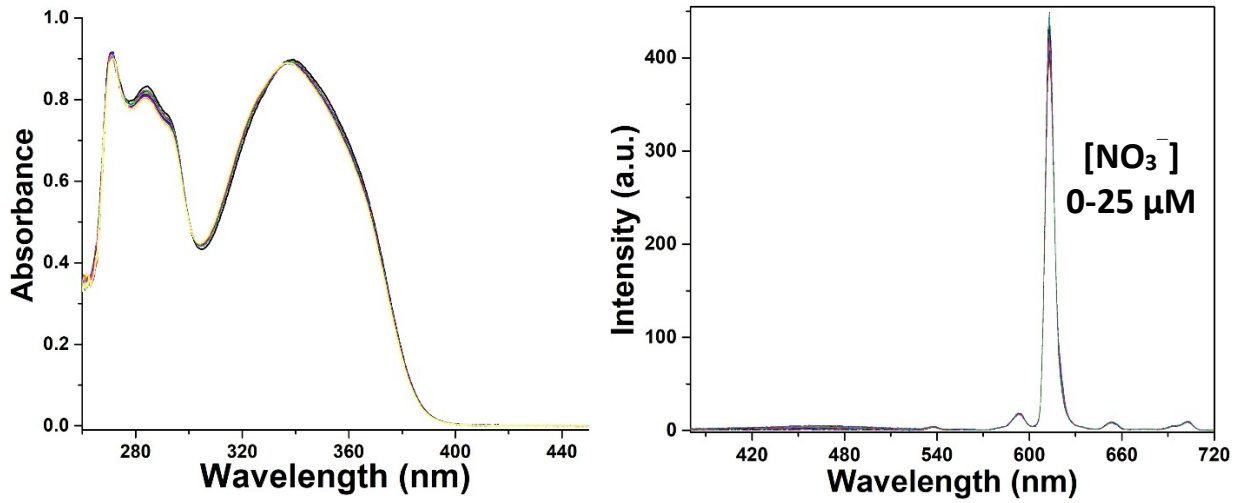

Fig. S16 Change in absorption spectra **(a)** and in the PL spectra **(b)** of **Eu.1** (2.5 µM) in MeCN with the increasing concentration of **[NO_3^-]** (0-25 µM, 0-10 equiv.) in H_2O observed at characteristic emissions of Eu(III) ($^5D_0 \rightarrow {}^7F_{J=0,1,2,3,4}$), λ_{ex} = 340 nm, ex. and em. slit width 5 nm.

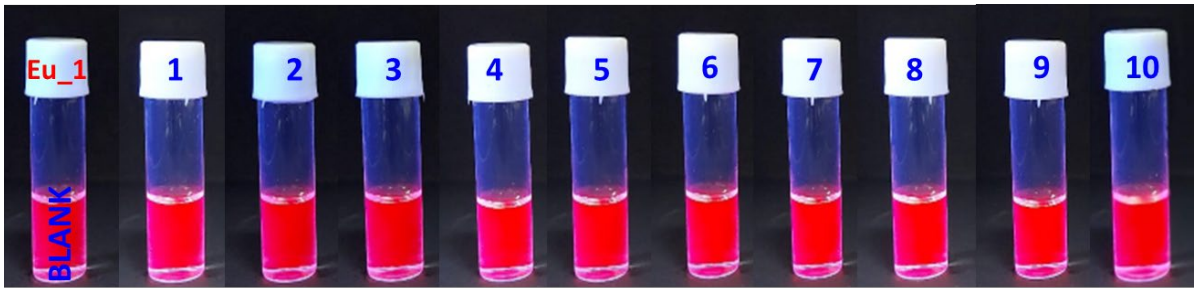

Fig. S17 Change in the emission of **Eu.1** (10 µM) in MeCN with the increasing concentration of **[NO_3^-]** in H_2O (0-100 µM, 0-10 equiv.) as seen from the naked eye under UV light (365 nm).

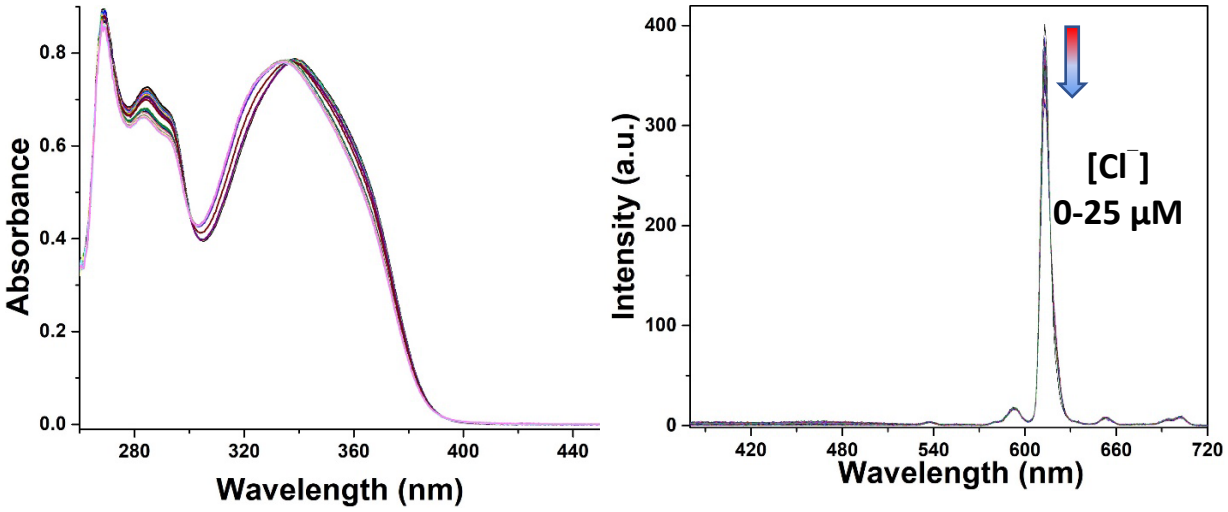

Fig. S18 Change in absorption spectra **(a)** and in the PL spectra **(b)** of **Eu.1** (2.5 µM) in MeCN with the increasing concentration of **[Cl⁻]** (0-25 µM, 0-10 equiv.) in H_2O observed at characteristic emission bands of Eu(III) ion ($^5D_0 \rightarrow {}^7F_{J=0,1,2,3,4}$), λ_{ex} = 340 nm, ex. and em. slit width 5 nm.

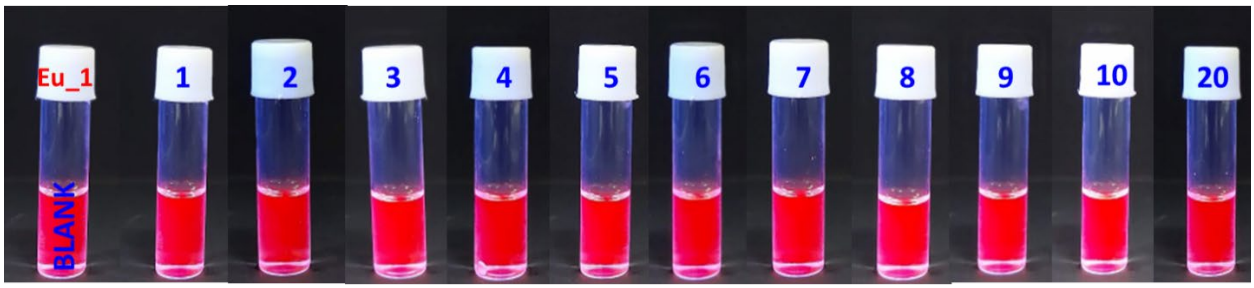

Fig. S19 Change in the emission of **Eu.1** (10 µM) in MeCN with the increasing concentration of **[Cl⁻]** in H_2O (0-200 µM, 0-20 equiv.) as seen from the naked eye under UV light (365 nm).

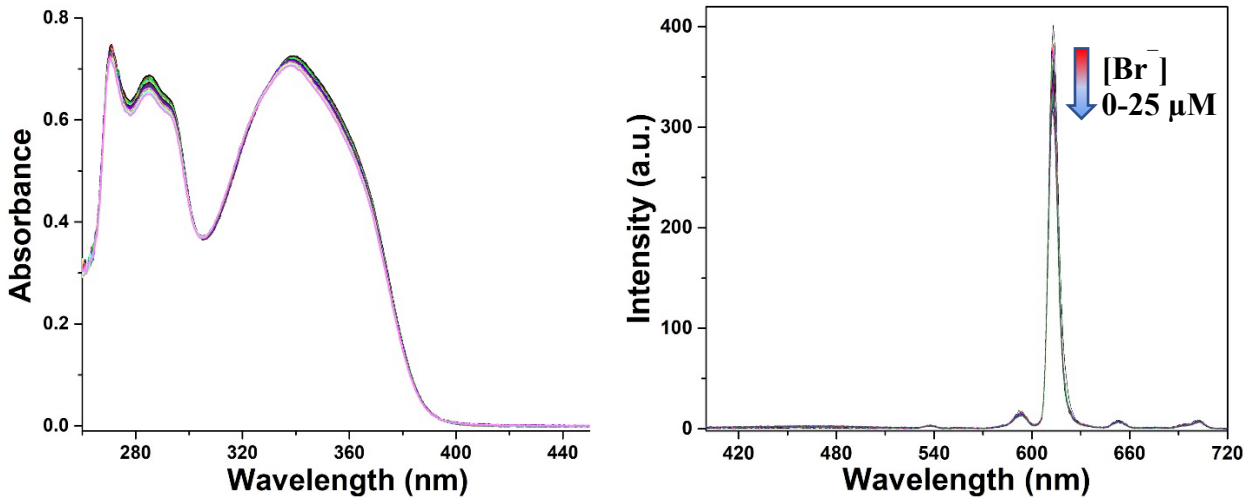

Fig. S20 Change in absorption spectra **(a)** and in the PL spectra **(b)** of **Eu.1** (2.5 µM) in MeCN with the increasing concentration of **[Br⁻]** (0-25 µM, 0-10 equiv.) in H_2O observed at characteristic emission bands of Eu(III) ($^5D_0 \rightarrow {}^7F_{J=0,1,2,3,4}$), λ_{ex} = 340 nm, ex. / em. slit width 5 nm.

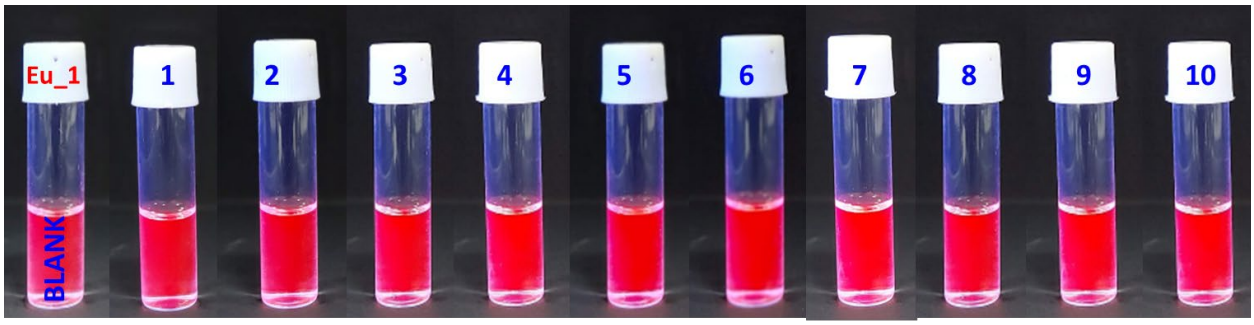

Fig. S21 Change in the emission of **Eu.1** (10 µM) in MeCN with the increasing concentration of **[Br⁻]** (0-100 µM, 0-10 equiv.) in H_2O as seen from the naked eye under UV light (365 nm).

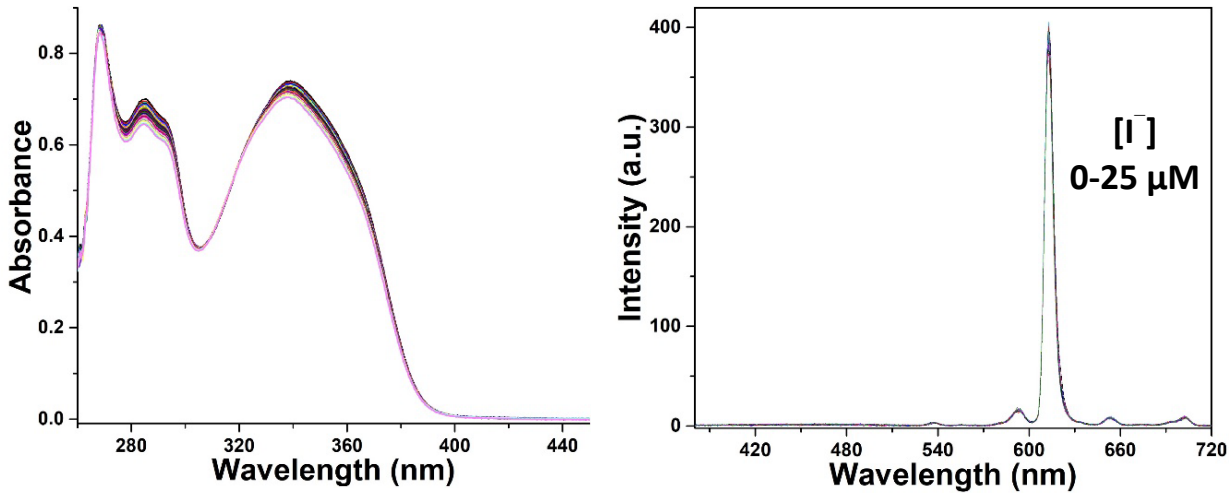

Fig. S22 Change in absorption spectra **(a)** and in the PL spectra **(b)** of **Eu.1** (2.5 µM) in MeCN with the increasing concentration of **[I⁻]** (0-25 µM, 0-10 equiv.) in H_2O observed at characteristic emission bands of Eu(III) ion ($^5D_0 \rightarrow {}^7F_{J=0,1,2,3,4}$), λ_{ex} = 340 nm, ex. and em. slit width = 5 nm.

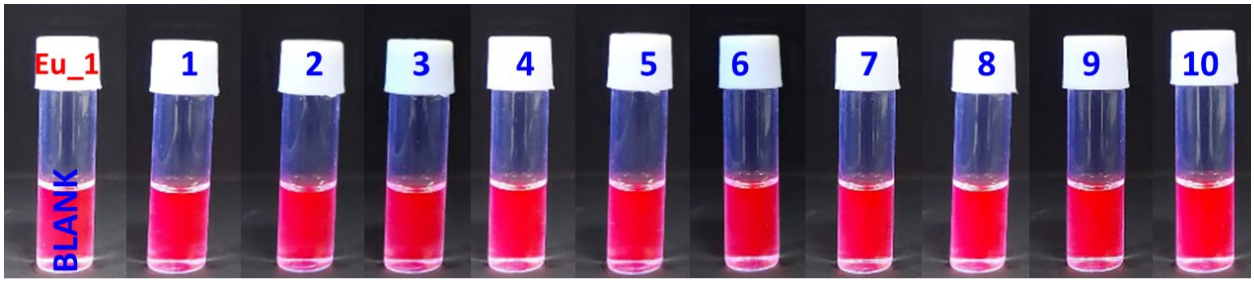

Fig. S23 Change in the emission of **Eu.1** (10 µM) in MeCN with the increasing concentration of **[I⁻]** (0-100 µM, 0-10 equiv.) in H_2O as seen from the naked eye under UV light (365 nm).

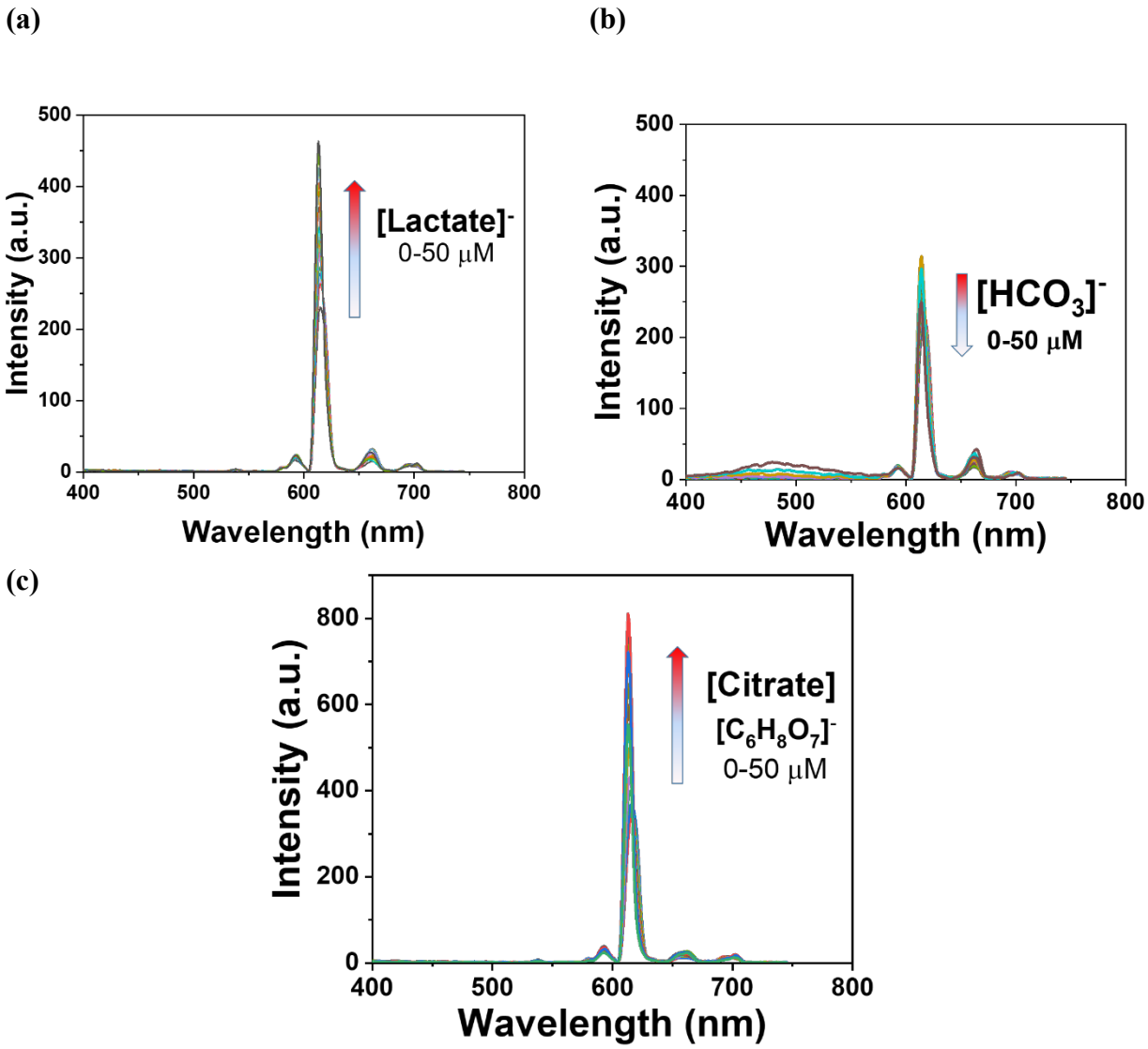

Fig. S24 Change in emission spectra of **Eu.1** (2.5 μM) on continuous addition of **(a)** lactate **(b)** bicarbonate [HCO_3^-], and **(c)** citrate (0-50 μM in MeCN:Water–75:25 (v/v), 0-20 equiv.) observed at characteristic emission bands of Eu(III) ion ($^5D_0 \rightarrow {}^7F_{J=0,1,2,3,4}$), $\lambda_{ex.}$ = 340 nm, ex. and em. slit width 5 nm.

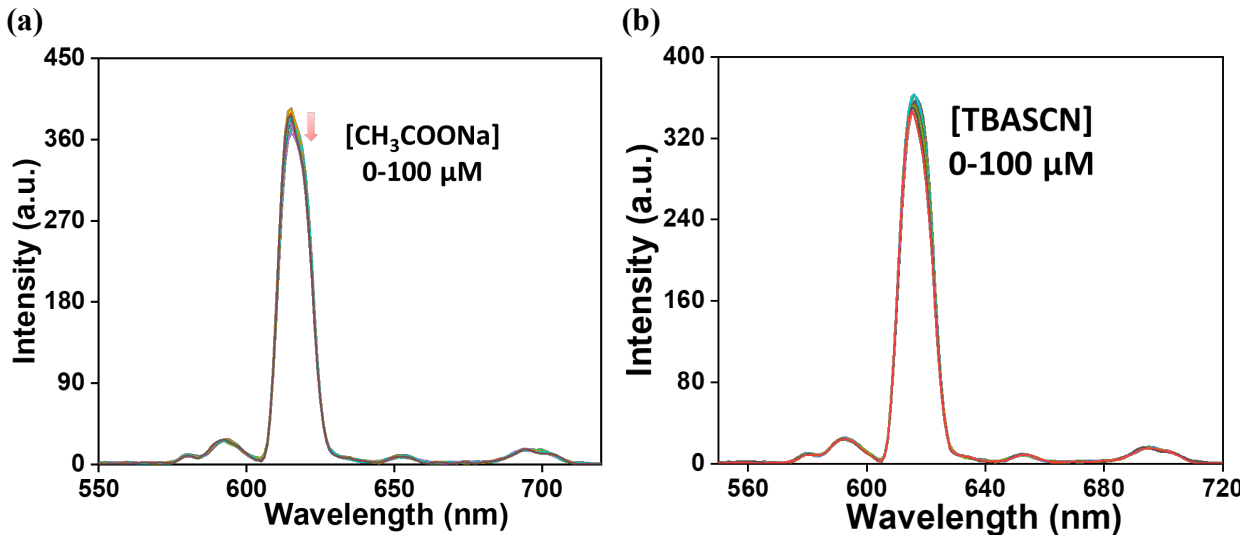

Fig. S25 Change in emission spectra of **Eu.1** (2.5 µM) on continuous addition of **(a)** CH_3COONa **(b)** TBASCN (in MeCN:Water–75:25 v/v) observed`(0-100 µM) at characteristic emission bands of Eu(III) ion ($^5D_0 \rightarrow {}^7F_{J=0,1,2,3,4}$), $\lambda_{ex.}$ = 340 nm, ex. and em. slit width = 5 nm.

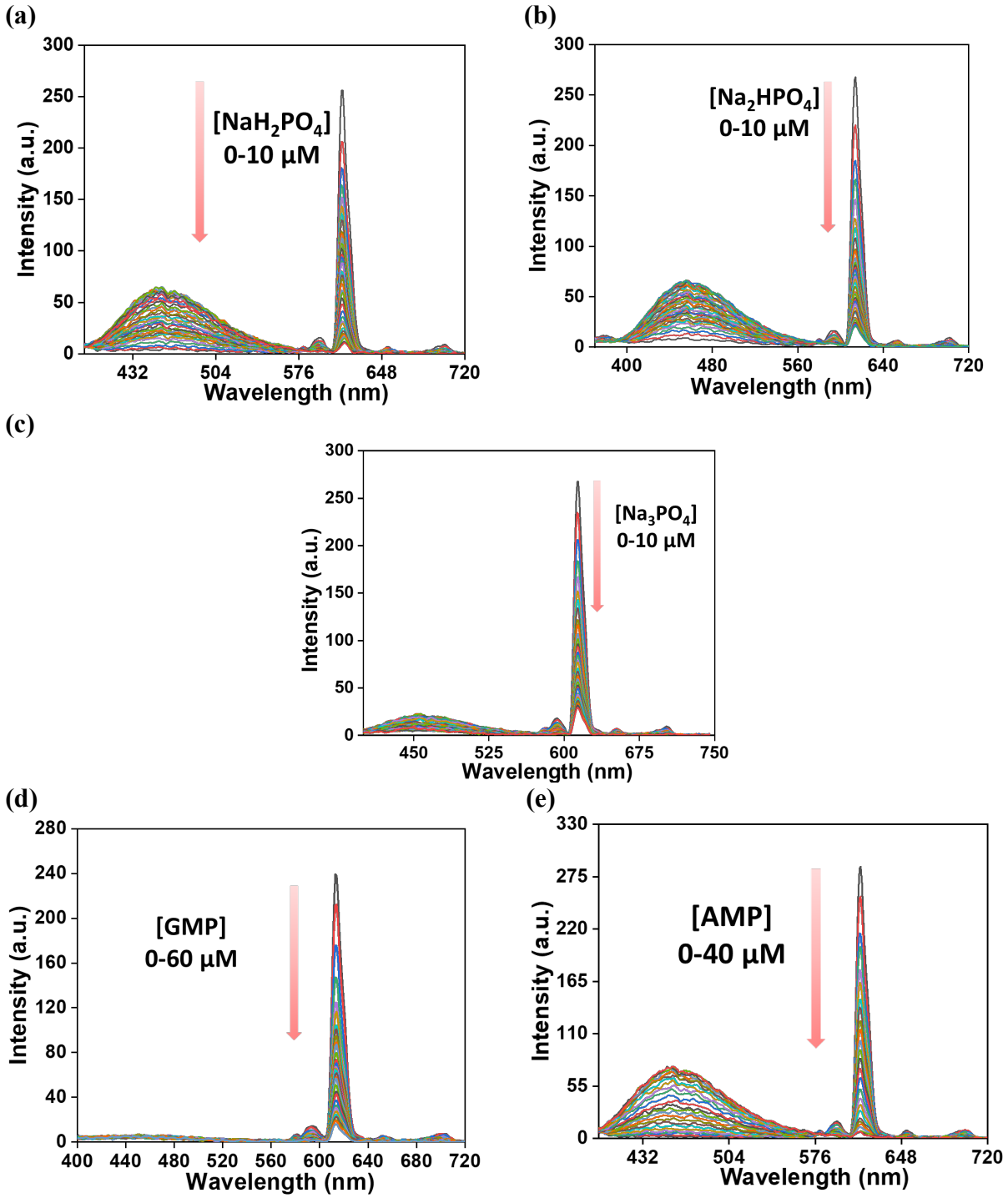

Fig. S26 Change in emission spectra of **Eu.1** (2.5 µM) on continuous addition of **(a) NaH_2PO_4 (b) Na_2HPO_4 (c) Na_3PO_4** (0-10 µM) and nucleotide phosphates **(d)** GMP (0-60 µM) **(e)** AMP (0-40 µM) as representative physiological phosphates in MeCN:Water–50:50, observed at characteristic emission bands of **Eu(III)** ion ($^5D_0 \rightarrow {}^7F_{J=0,1,2,3,4}$), $\lambda_{ex.}$ = 340 nm, ex. and em. slit width 5 nm.

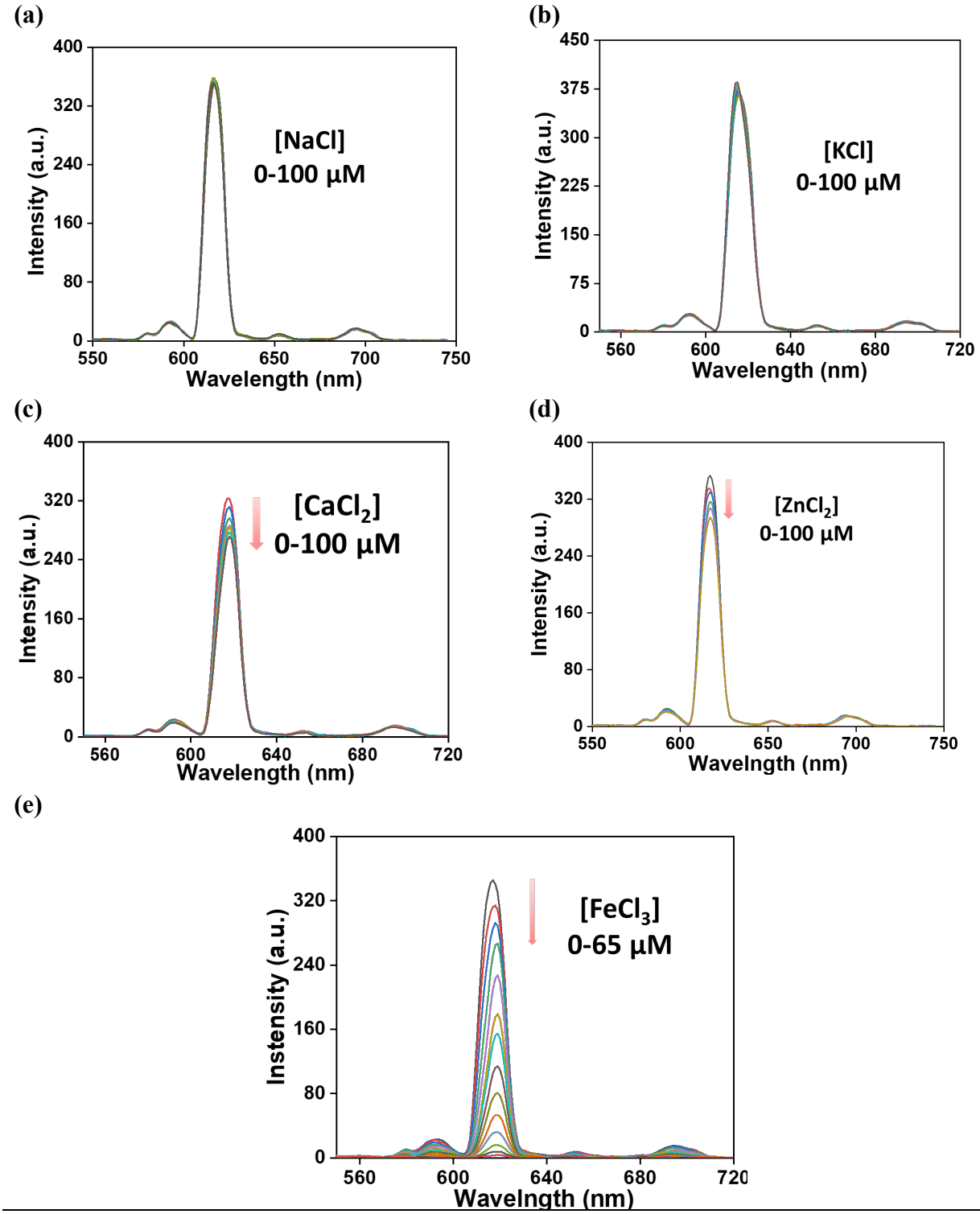

Fig. S27 Changes in emission spectra of **Eu.1** (2.5 µM) on continuous addition of (a) NaCl (b) KCl (c) $CaCl_2$ (d) $ZnCl_2$ (e) $FeCl_3$ (MeCN:Water–75:25) observed at characteristic emission bands of Eu(III) ion ($^5D_0 \rightarrow {}^7F_{J=0,1,2,3,4}$), $\lambda_{ex.}$ = 340 nm, ex. and em. slit width 5 nm.

(a)

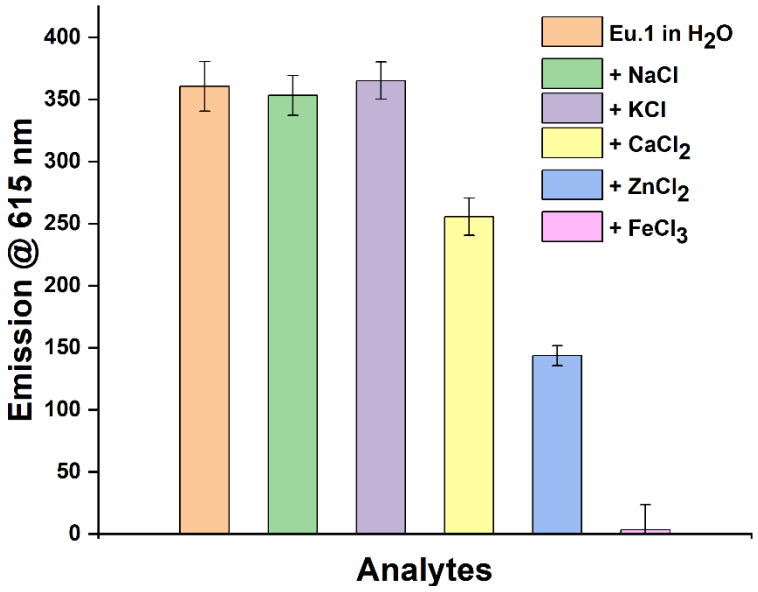

Fig. S28 Bar plot representing the emission intensity at 615 nm from **Eu.1** on addition of different metal ions (0-75 μM, each) in MeCN:Water (75:25 v/v), $\lambda_{ex.}$ = 340 nm, ex. and em. slit width 5 nm.

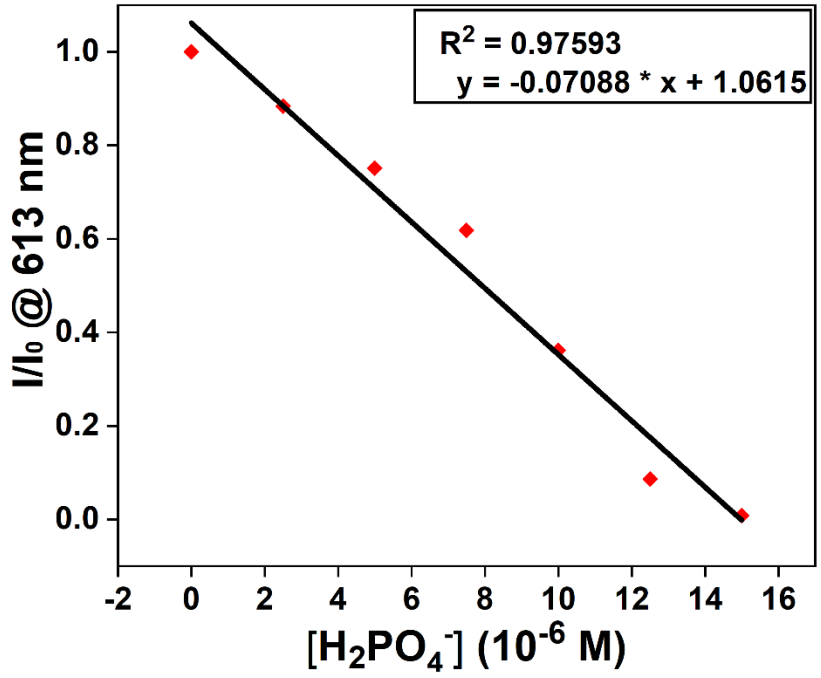

Fig. S29 Plot for the calculation of limit of detection (LOD) of phosphate ion plotted for 613 nm with the continuous addition of the $H_2PO_4^-$.

Limit of Detection Calculations:

LOD = 3.3 σ/*s*

Where, **σ** is the standard deviation of the regression line and ***s*** is the slope of the curve.

For **Eu.1**, ***s*** = 0.07088 and **σ** = 0.38748

LOD = 18 ppb

[Eu.1] - L^{N4}

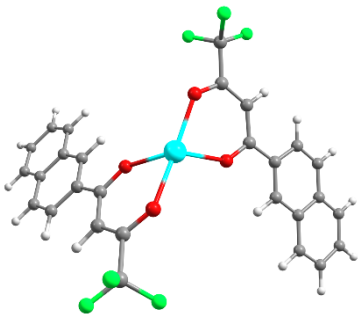

dEu-O(tfnb) = 2.197-2.198

[Eu.1]- L^{N4} + 2[$H_2PO_4^-$]

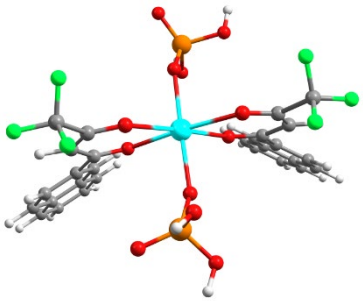

dEu-O(tfnb) = 2.363-2.378

dEu-O($H_2PO_4^-$) = 2.261

[Eu.1]- L^{N4}+ [$H_2PO_4^-$] + H_2O

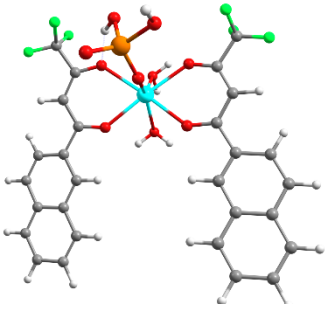

dEu-O(tfnb) = 2.348-2.385

dEu-O($H_2PO_4^-$) = 2.245

dEu-O(H_2O) = 2.525-2.576

[Eu.1]- L^{N4}+ 2[$H_2PO_4^-$] + 2H_2O

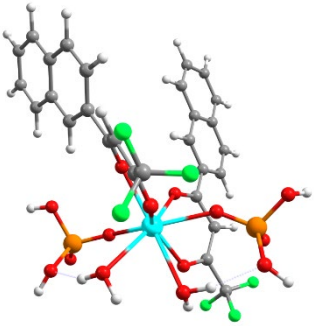

dEu-O(tfnb) = 2.280-2.538

dEu-O($H_2PO_4^-$) = 2.280-2.329

dEu-O(H_2O) = 2.483-2.618

[Eu.1]- L^{N4}+ 2[$H_2PO_4^-$] + 2H_2O (Chain)

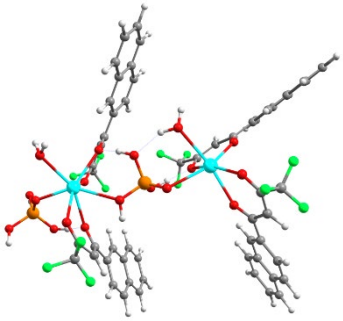

dEu-O(tfnb) = 2.352-2.648

dEu-O($H_2PO_4^-$) = 2.463-2.908

dEu-O(H_2O) = 2.602-2.666

Eu.1]- L^{N4}+ 2[$H_2PO_4^-$] + 2H_2O (Bridge)

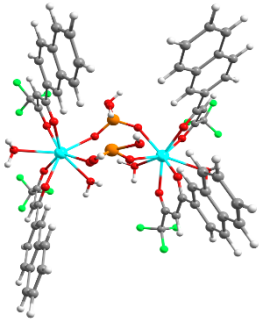

dEu-O(tfnb) = 2.288-2.394

dEu-O($H_2PO_4^-$) = 2.319-2.530

dEu-O(H_2O) = 2.513-2.644

Fig. S30 DFT-optimized molecular structures of **Eu.1** bound to phosphate(s) in different binding modes/speciations (after dissociation of L^{N4}). Some general bond lengths (theoretical) have been reported below the structures.

S31. Quantum Yield:

The quantum yield (ϕ_x) was calculated by using relative quantum yield measurement using the formulae:

$$\phi_x = \left(\frac{A_R}{Ax}\right)\left(\frac{E_x}{E_R}\right)\left(\frac{n_x}{n_R}\right)^2 \phi_R$$

Where Φ is the luminescence quantum yield, A is the absorbance at the excitation wavelength, E is the area under the corrected emission curve (expressed in number of photons), n is the refractive index of the solvents used. The subscripts R and X refer to the reference and the unknown samples respectively. The ideal absorbance value was kept around 0.2 to keep the emission intensity directly proportional to the concentration of the analyte. $Cs_3[Eu(DPA)_3]$ was used as an internal standard with Φ_R = 13.5% ± 1.5% in 0.1 M tris buffer at pH 7.0.

Area Under the curve for Reference = 1985.53

Area under the curve for **Eu.1** = 1484.54

n_x = 1

n_R = 1.3

***ϕ_x = 5.97 ± 1.5 in water at $\lambda_{ex.}$* = 279 nm.**